This is a repository copy of *Near-wall interparticle collision dynamics in multi-phase turbulent channel flows*.

White Rose Research Online URL for this paper:
http://eprints.whiterose.ac.uk/134971/

Version: Accepted Version

Proceedings Paper:
Mortimer, LF, Fairweather, M and Njobuenwu, DO orcid.org/0000-0001-6606-1912 (2018) Near-wall interparticle collision dynamics in multi-phase turbulent channel flows. In: Proceedings of the Ninth International Symposium on Turbulence, Heat and Mass Transfer. Turbulence, Heat and Mass Transfer 9, 10-13 Jul 2018, Rio de Janeiro, Brazil. Begell House Inc , pp. 807-818. ISBN 978-1-56700-468-7

This is an author produced version of a conference paper published in Proceedings of the Ninth International Symposium On Turbulence, Heat and Mass Transfer. Uploaded in accordance with the publisher's self-archiving policy.

Near-wall interparticle collision dynamics in multi-phase turbulent channel flows

L.F. Mortimer, M. Fairweather and D.O. Njobuenwu

School of Chemical and Process Engineering, University of Leeds, Leeds LS2 9JT, UK

pmlfm@leeds.ac.uk; m.fairweather@leedsac.uk; d.o.njobuenwu@leeds.ac.uk

Abstract – Interparticle collision statistics in a turbulent channel flow are obtained using direct numerical simulation coupled to Lagrangian particle tracking. The particle motion solver considers drag, lift, pressure gradient and added mass force contributions. Fluid momentum coupling and hard-sphere deterministic interparticle collisions are also accounted for. Collision behaviour for particle Stokes numbers outside of the range usually considered in similar investigations is discussed in detail. The analysis focuses on separating the turbulent channel flow into four regions of varying turbulence intensity. Collision velocities are analysed for each region and discussion as to how particles obtain those velocities is offered. The mean value of the collision angle is observed to scale with both Stokes number and wall proximity, with the former having the greatest effect. The greatest collision rate is found to be in the viscous sublayer and for the higher Stokes number.

1. Introduction

The dynamics surrounding particle behaviour in turbulent multi-phase flows are of interest in many industrial processes and applications. For instance, the chemical manufacture and mineral processing industries all require an understanding of flow properties when particles possessing certain characteristics are dispersed throughout a turbulent system. This work focuses on applications within nuclear reactor coolant and waste processing flows, in which interparticle interactions such as collision and agglomeration are of importance and have been observed to impact on the safety and performance of the system. An example is the build-up of CRUD (Chalk River unidentified deposits) [1], which are deposits of agglomerated particles on reactor cladding fuel pins which can lead to poor heat transfer conditions and promote local corrosion. In such systems, particles are likely to encounter regions of turbulence due to the presence of moderate to high flow rates. To be able to understand and predict these types of flows would be invaluable in maintaining coolant and reactor efficiency.

Single-phase experimental and computational studies of wall-bounded turbulence have provided a good understanding of the continuous phase flow topology and dynamics. For instance, vortical structures have been observed and categorized via various regimes. Blackburn et al. [2] and Chong et al. [3] use velocity gradient tensor invariants to characterise vortices in incompressible flows. Probability density functions of these invariants differ throughout each region of the channel flow, indicating various turbulence structures.

Multi-phase flow investigations via simulation have also been performed due to increases in computing power over the past decade. Many works choose to consider a range of particle Stokes number, $St^+ = \tau_P/\tau_F$, which relates the relaxation time of the particle, $\tau_P = \rho_P d_P^2/18\rho_F \nu_F$, to the viscous timescale associated with the flow, $\tau_F = \nu_F/u_\tau^2$. Here, ρ_F and ρ_P are the density of the continuous and discrete phases, respectively, d_P is the diameter of the particle, ν_F is the kinematic viscosity of the

fluid and u_τ is the shear velocity of the fluid. At low Stokes numbers ($St^+ < 1$), particles behave like tracers and follow the continuous phase streamlines. With increased Stokes number, particle motion decouples from that of the flow and is dominated by inertia. An important phenomenon in wall-bounded flows is turbophoresis [4], which is the drift of particles towards the wall induced by turbulence. This leads to an eventual build-up of particles very close to the solid boundary, an effect more enhanced at larger Stokes numbers [5]. Furthermore, upon reaching the near-wall region, authors have observed particles of moderate Stokes number ($St^+ \sim 25$) collecting in low-speed streaks, leading to an increased local particle concentration and hence larger interaction cross section. Rouson and Eaton [6] observed a variety of dynamic particle responses to dispersion in the vicinity of the previously mentioned turbulence structures, and so the channel flow region inevitably plays an important role in determining collision behaviour.

At high enough volume fractions or local concentrations, particles will interact often enough such that the behaviour of both phases changes from that of a one-way coupled system. Elghobashi [7] suggests that the regime in which both fluid-particle momentum coupling and particle collisions must be considered is at solid phase volume fractions around $\phi_P \sim 10^{-3}$, and even lower for particles with large Stokes numbers. Recent studies demonstrated that interparticle behaviours differ depending on the intensity and type of turbulence structures that they encounter, which in channel flows includes a dependence on the proximity to the wall boundary. For instance, Bäbler et al. [8] observed experimentally that collision rates were increased as a result of local turbulence in dispersed particle-fluid flows. To perform simulations with such dynamics, either a deterministic or stochastic collision model is required. Tanaka and Tsuji [9] performed a computational study in a short pipe element with few, relatively large particles. They observed an isotropisation of the root mean square (rms) of velocity fluctuations upon allowing for interparticle collisions. Oesterle and Petitjean [10] developed a stochastic model, which relies on radial distribution functions, although in general these are not easy to obtain. The findings of such studies include that turbulence intensities are dampened by inertial particles with increasing volume fraction [11]. Turbulence isotropisation has been further predicted by later works [12] and turbophoresis has been observed to be reduced due to particle collisions [13]. These investigations provide a strong foundation on which to build understanding surrounding the physics of particle-fluid and particle-particle interactions in turbulent flows.

The present work aims to elucidate the particle-particle interaction dynamics in each region of a turbulent channel flow by performing simulations which couple both the fluid and particle phases with high accuracy numerical solvers. Collisions are handled in a deterministic manner, using a fully elastic hard sphere model for post-collision momenta. A grid search algorithm is implemented to reduce the number of computations necessary to detect a collision event. The properties of each phase have been chosen to resemble the flow of glass particles in a relatively viscous liquid such as water, and that of a gaseous phase such as air. Each Stokes number considered is obtained by fixing the particle diameter (corresponding to a $100\,\mu m$ particle in a $40\,mm$ height channel), and varying the particle-fluid density ratio $\rho_P^* = \rho_P / \rho_F$. The analysis below includes various collision information such as relative rebound velocities and angles.

2. Methodology

The motion of particles through a turbulent channel flow is simulated using Lagrangian particle tracking (LPT) coupled with the fluid-phase solver, Nek5000 (https://nek5000.mcs.anl.gov/). The nature of the study requires that solid-phase trajectories are calculated to high accuracy. As such, direct numerical simulation (DNS) is utilized to obtain a flow-field which resolves all relevant turbulence length and timescales. Nek5000 uses a high-order spectral element method, and has been chosen based upon its parallelisation capabilities, scalability, and its testing and validation history.

The governing equations for the continuous phase are the Navier-Stokes equations in dimensionless incompressible form:

$$\boldsymbol{\nabla} \cdot \boldsymbol{u}^* = 0, \tag{1}$$

$$\frac{D\boldsymbol{u}^*}{Dt^*} = -\boldsymbol{\nabla}p^* + \frac{1}{Re_B}\nabla^2\boldsymbol{u}^* + \boldsymbol{f}^*_{PG} + \boldsymbol{f}^*_{2W}, \tag{2}$$

where $\boldsymbol{u}^*$ represents the fluid velocity vector, p^* the fluid pressure, Re_B the bulk flow Reynolds number ($Re_B = U_B\delta/\nu_F = 2800$), ν_F the fluid kinematic viscosity, and where $\boldsymbol{f}^*_{PG}$ a constant pressure gradient flow forcing term. These quantities are non-dimensionalised using the channel half-height, δ, the bulk velocity, U_B, and the fluid phase density, ρ_F. Any quantity labelled with an asterisk (*) denotes a variable non-dimensionalised in this manner. $\boldsymbol{f}^*_{2W}$ is cell dependent and represents the two-way coupling term which models the influence of the particle's momentum feedback on the fluid.

The solution domain consists of a Cartesian discretized grid made up of 27 × 18 × 23 7th order elements, used to represent a 12δ × 2δ × 6δ channel in the streamwise, wall-normal and spanwise directions, respectively. Elements close to the wall are more densely distributed to provide increased resolution in the turbulent regions. The wall-normal direction uses no-slip and impermeability conditions at the walls ($y^* = \pm 1$), and the remaining two directions enforce periodic boundary conditions. A constant pressure gradient drives and maintains the flow in the streamwise direction, ensuring a shear Reynolds number of $Re_\tau = u_\tau\delta/\nu_F$ = 180, where u_τ is the shear velocity, given by $u_\tau = \sqrt{\tau_W/\rho_F}$, with τ_W the mean wall shear stress. Thus:

$$\boldsymbol{f}^*_{PG} = \frac{\partial p^*}{\partial x^*}\hat{x} = \left(\frac{Re_\tau}{Re_B}\right)^2 \hat{x}, \tag{3}$$

where $\hat{x}$ is a unit vector in the streamwise direction. The computational domain setup is illustrated in Figure 1.
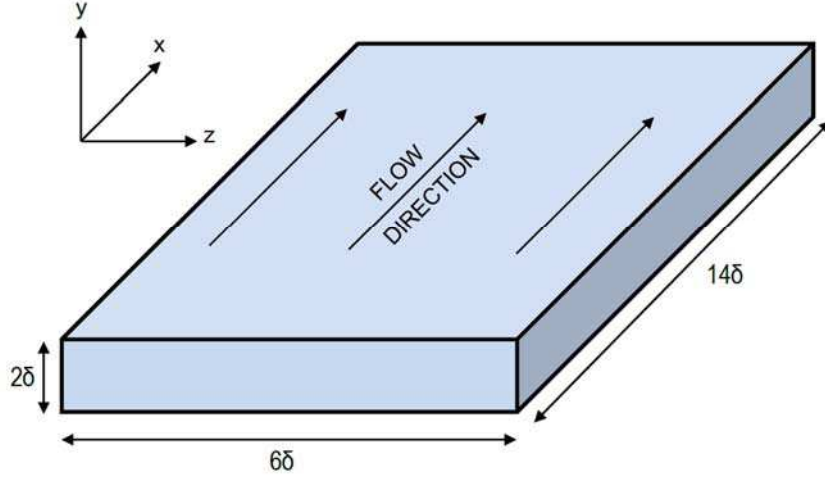
Figure 1: Schematic of turbulent channel flow computational domain.

The LPT interfaces concurrently with the DNS solver. Particles are represented by small, undeformable computational spheres. After an Eulerian timestep is performed, the LPT solves the non-dimensional Newtonian equations of motion for each particle to calculate changes in velocity and displacement. These equations derive from the force-balance between the particle's inertia and perturbations due to the fluid. For this study, both small and large density ratios are investigated. As such, contributions from Saffman lift, pressure gradient and added mass forces are included:

$$\frac{\partial \boldsymbol{x}_P^*}{\partial t^*} = \boldsymbol{u}_P^*, \tag{4}$$

$$\frac{\partial \boldsymbol{u}_P^*}{\partial t^*} = \frac{1}{M_{VM}} \left[\underbrace{\frac{3C_D |\boldsymbol{u}_s^*|}{4 d_p^* \rho_P^*} \boldsymbol{u}_s^*}_{Drag} + \underbrace{\frac{3}{4} \frac{C_L}{\rho_P^*} (\boldsymbol{u}_s^* \times \boldsymbol{\omega}_F^*)}_{Lift} + \underbrace{\frac{1}{2\rho_P^*} \frac{D' \boldsymbol{u}_F^*}{Dt^*}}_{Added\ mass} + \underbrace{\frac{1}{\rho_P^*} \frac{D \boldsymbol{u}_F^*}{Dt^*}}_{Pressure\ gradient} \right]. \tag{5}$$

Here, $\boldsymbol{x}_P^*$ is the particle position, $\boldsymbol{u}_P^*$ the particle velocity, $\boldsymbol{u}_F^*$ the spectrally interpolated fluid velocity at the particle position, $\boldsymbol{u}_s^* = \boldsymbol{u}_F^* - \boldsymbol{u}_P^*$ the slip velocity, d_P^* the non-dimensional particle diameter, ρ_P^* the density ratio of the particle to the fluid and $\boldsymbol{\omega}_F^*$ the fluid vorticity, where $\boldsymbol{\omega}_F^* = \nabla \times \boldsymbol{u}_F^*$. The drag coefficient, C_D, is taken from the empirical observations of Schiller and Naumann [14] such that $C_D = 24 f_D / Re_P$, where $f_D = (1 + 0.15 Re_P^{0.687})$ when $Re_P > 0.5$, else $f_D = 24 / Re_P$. Here, Re_P is the particle Reynolds number, given by $Re_P = Re_B d_P^* |\boldsymbol{u}_s^*|$. The expression for shear lift force uses the Saffman-Mei coefficient, C_L [15, 16]. The derivative $D'/Dt^* = \partial/\partial t + \boldsymbol{u}_P \cdot \nabla$ is used to obtain the acceleration of the fluid as observed by the particle. D/Dt^* is the material derivative with respect to the moving flow. M_{VM} is the virtual mass modification term, $M_{VM} = (1 + \frac{1}{2\rho_P^*})$.

Upon completion of a continuous phase timestep, the required flow field parameters $(\boldsymbol{u}_F^*, \boldsymbol{\omega}_F^*, \frac{D\boldsymbol{u}_F^*}{Dt^*})$ are obtained via spectral interpolation. Eqs. (4) and (5) are then solved using a fourth-order Runge-Kutta scheme, employing a solid-phase timestep ($\Delta t^* = 0.02$) equal to that of the fluid-phase solver.

Each particle's inertial effect on the fluid phase was considered through the

inclusion of an additional source term in the Navier-Stokes equations as $\boldsymbol{f}^{*}_{2W} = -\frac{1}{V_{C}}\sum_{i=1}^{N_{P}}\frac{\partial \boldsymbol{u}^{*}_{P,i}}{\partial t^{*}}$, where V_{C} is the volume of the cell formed by the bisectors between two Gauss-Lobatto-Legendre points. This feedback term is the same formulation as presented in Squires and Eaton [17], with all particles acting as point forces.

Interparticle collisions were performed deterministically. The binary collision algorithm was run using a virtual homogeneous coarse mesh to search for collisions, reducing the cost of the search from $O(N_{P}^{2})$ to $O(N_{P})$, where N_{P} is the number of particles in the system. The mesh cells were small enough such that they contained few particles, but large enough that it is unlikely a particle would exit the cell during a given timestep. A standard collision search between all particles within a cell was performed to determine the occurrence of a collision event. If the magnitude of the relative particle positions was less than the sum of their radii after an advection step was performed, a collision was judged to occur.

To determine post-collision velocities, conservation of momentum was used with fully elastic collision dynamics (restitution coefficient $e = 1$). To increase accuracy, the time spent intersecting another particle was used to determine an initial rebound length, which was used to correct the new position of the particle after the collision was performed. Collisions with the wall were handled in a similar fashion, with reflection of the wall-normal component of particle velocity accounting for a smooth, fixed boundary.

The simulation parameters used in the present study are presented in Table 1.

Table 1: Simulation parameters.

Parameter	$St^{+} \approx 0.1$	$St^{+} \approx 92$
Shear Reynolds number	180	180
Bulk Reynolds number	2800	2800
Particle diameter, d_{P}^{*}	0.005	0.005
Particle diameter, d_{P}^{+}	0.9	0.9
Number of particles, N_{P}	300,000	300,000
Shear Stokes number, St_{τ}	0.11	91.84
Bulk Stokes number, St_{B}	0.01	7.94
Density ratio, ρ_{P}^{*}	2.5	2041
Volume fraction, Θ_{P}	10^{-4}	10^{-4}
Particle and fluid timestep, Δt^{*}	0.02	0.02
Particle and fluid timestep, Δt^{+}	0.23	0.23

Particle Stokes numbers were chosen such that they lie outside the regime where particle clustering in low-speed streaks occurs. This was in an effort to analyse more closely the effects of particle inertia and decorrelation from turbulence. The $St^{+} = 0.1$ particles behave like fluid tracers and could represent glass particles in water. The $St^{+} = 92$ particles are highly inertial and could represent glass particles in air. An initial simulation was run without particles to establish turbulence, and the fluid statistics were monitored periodically until the mean streamwise velocity and rms velocity fluctuations had reached a statistically steady state. Particles were then randomly injected throughout the channel domain, and given an initial velocity equal

to that of the interpolated fluid at their position. Each solver was run concurrently, with discrete phase statistics gathered once mean profiles were stationary.

3. Results and Discussion

Firstly, a validation for both the continuous phase solver and the LPT is provided. Figure 2 compares the single-phase fluid mean streamwise velocity and turbulence velocity fluctuations to those of the previous DNS results of Vremen and Kuerten [18], using the S2B3 dataset. Excellent agreement is obtained in both cases. There exists little experimental or computational data for particle-laden flows at $Re_\tau = 180,$ and so a multi-phase simulation was performed at a slightly lower Reynolds number in an effort to validate the LPT. Figure 3 was obtained from a separate simulation performed at $Re_\tau = 150$ and $St^+ = 1$, matching the parameters and setup of Marchioli et al. [19]. Validation data is taken from the TUE dataset and, overall, very good agreement is shown. It is noticed that there appears to be a slight over-prediction of the streamwise rms velocity fluctuations close to the wall, however there existed a spread of values for this quantity in the databases in [19], and so some deviation is to be expected. It is important to note that in these validation simulations, solely drag forces were considered in the force balance equation. Both phases show strong agreement with the other simulations noted which builds confidence in the overall model and the findings of the simulations at the higher Reynolds number.
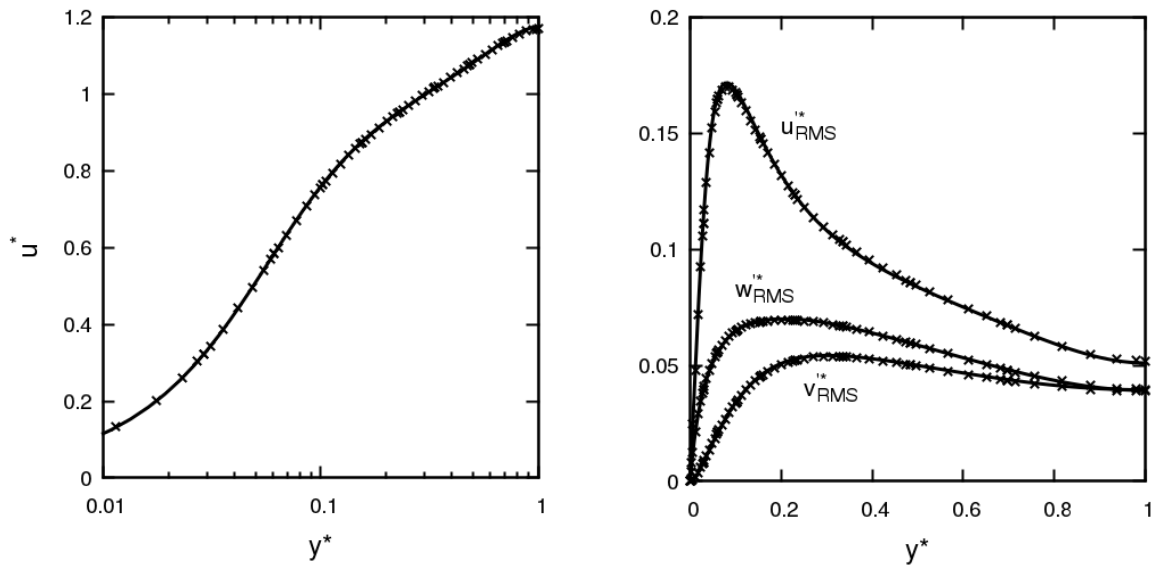

Figure 2: Mean streamwise velocity (left) and rms of velocity fluctuations (right) for continuous phase at $Re_\tau = 180$, crosses – present, lines – Vremen and Kuerten [18].
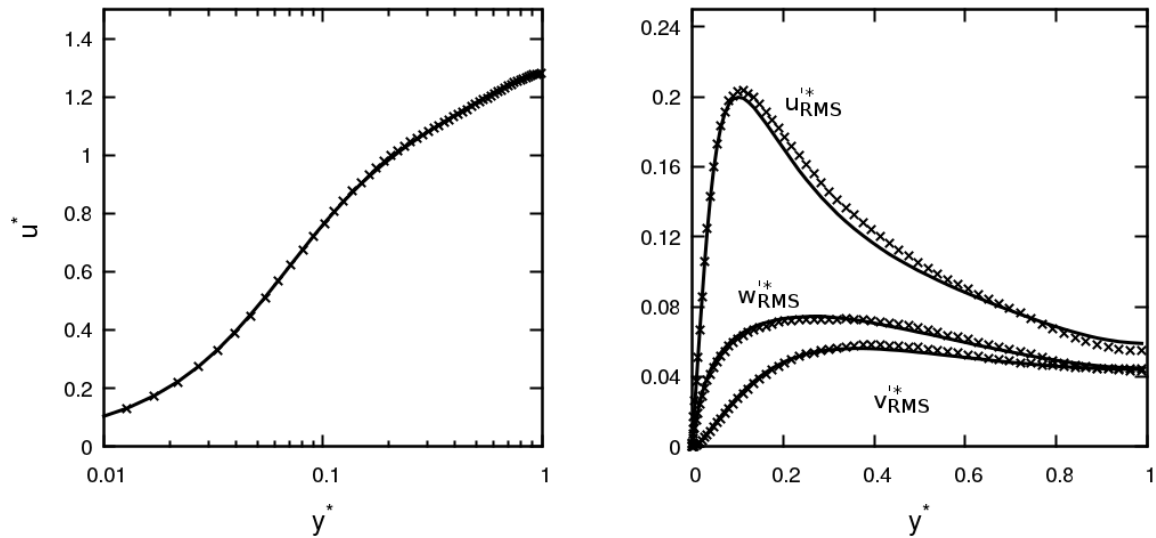
Figure 3: Mean streamwise velocity (left) and rms of velocity fluctuations (right) for particulate phase at $Re_\tau = 150$ and $St^+ = 1$, crosses – present, lines – Marchioli et al. [19].

For the analysis presented, collisions occurring within four distinct regions of the channel were considered. The four regions are: the viscous sublayer ($0 \leq y^* < 0.027$), the buffer layer ($0.027 \leq y^* < 0.166$), the log-law region ($0.166 \leq y^* \leq 0.2$) and the bulk flow region ($0.2 \leq y^* \leq 1$). These layers are mirrored about the channel centreline ($y^* = 1$).

Statistics surrounding collision events were generated in an effort to elucidate the way in which collisions occur. Figure 4 illustrates the mean concentration profiles for each simulation, obtained during the interval $100 < t^* < 150$. It is clear here that turbophoretic effects are much more apparent at $St^+ = 92$ which agrees with previous findings. The relative concentrations are important since the local volume fraction in the near-wall region will increase for the larger Stokes number. This means inter-particle collisions will be more likely to affect the fluid and solid phase flow properties. Since turbophoresis encourages particles in the direction of decreasing turbulence kinetic energy, a slight increase in the bulk is observed at high Stokes number for particles remaining close to the channel centre.
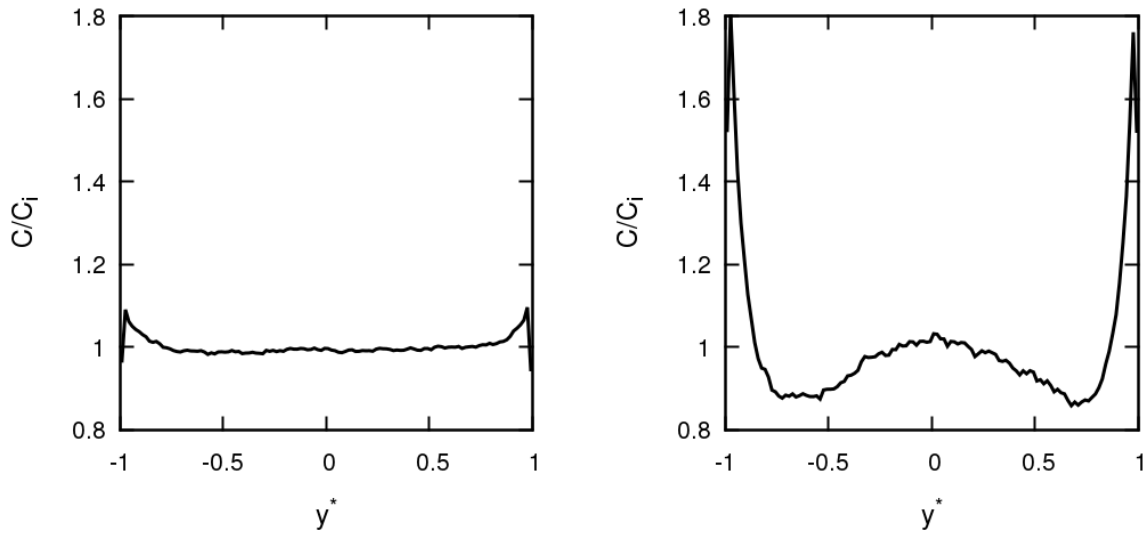
Figure 4: Mean particle concentration profiles normalized by initial concentration at $St^+ = 0.1$ (left) and $St^+ = 92$ (right). Profiles were obtained starting from $t^* = 100$ and averaged over a sample interval of length $t^*_{AVG} = 50$.

Figures 5 to 7 illustrate probability density functions (PDFs) of particle velocity components before a collision takes place. These were gathered after the system reached a statistically steady state, based on averaged flow properties such as those demonstrated in the validation.

Figure 5 (streamwise velocity of colliders) indicates that the greatest spread of collision velocities is within the buffer layer for both low and high Stokes numbers. An interesting observation is that particles with low Stokes numbers have much more well defined streamwise velocities in the viscous sublayer, whereas the range is almost doubled for highly inertial particles. This can be explained by the fact that particles at $St^+ = 92$ are highly decorrelated from the turbulence field, and so have an increased chance of inter-region migration whilst retaining their velocity. This mechanism would indeed increase the spread of velocities, particularly in the near-wall regions. On the other hand, streamwise collision velocities in the bulk are very similar.

Considering wall-normal particle velocities (Fig. 6), the greatest spread of this quantity is in the bulk and log-law regions for low Stokes particles, whereas collisions closer to the wall are more defined. The opposite is true for inertial particles, where the greatest spread lies within the near-wall regions. Given the increased concentration and turbulence decorrelation in this region, and increased likelihood of wall collisions due to particle inertia, this observation is unsurprising.

Figure 7 shows the relative spanwise velocities between the colliding particle and that of its neighbour before the collision takes place. For the larger Stokes number, the behaviour is similar to that of the wall-normal component, whereby the three regions nearest the wall have particles colliding with a very similar distribution of velocities. Again, bulk collisions favour lower spanwise velocities. For low Stokes number particles, the greatest spread of spanwise velocities is in the log-law region, yet particles in the viscous sublayer have more well defined spanwise speeds.
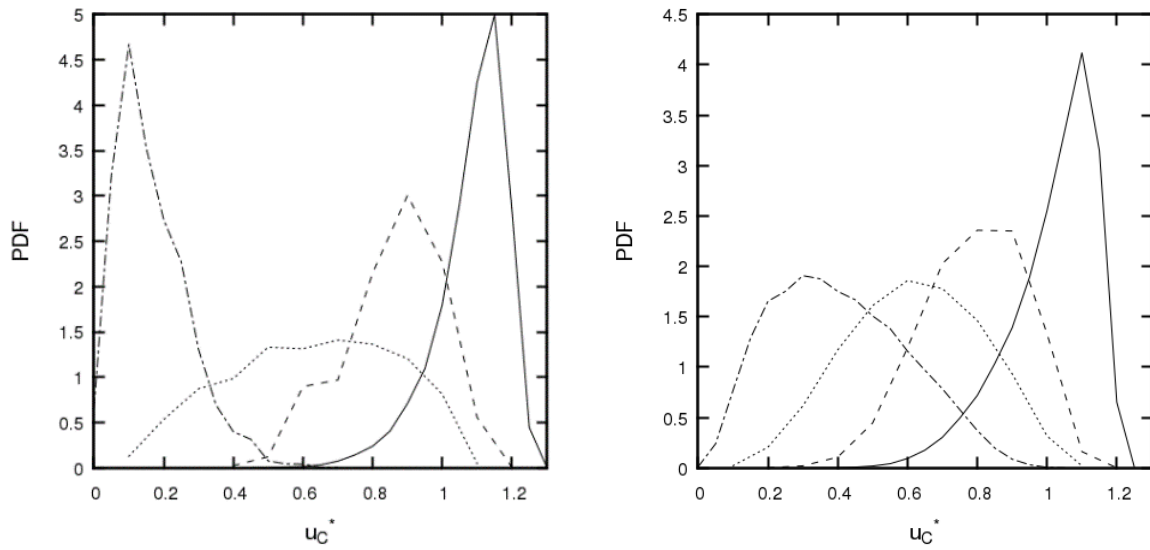
Figure 5: PDFs of collider streamwise velocity at $St^+ = 0.1$ (left) and $St^+ = 92$ (right). Solid line: bulk flow; dashed: log-law region; dotted: buffer layer; dot-dashed: viscous sublayer.
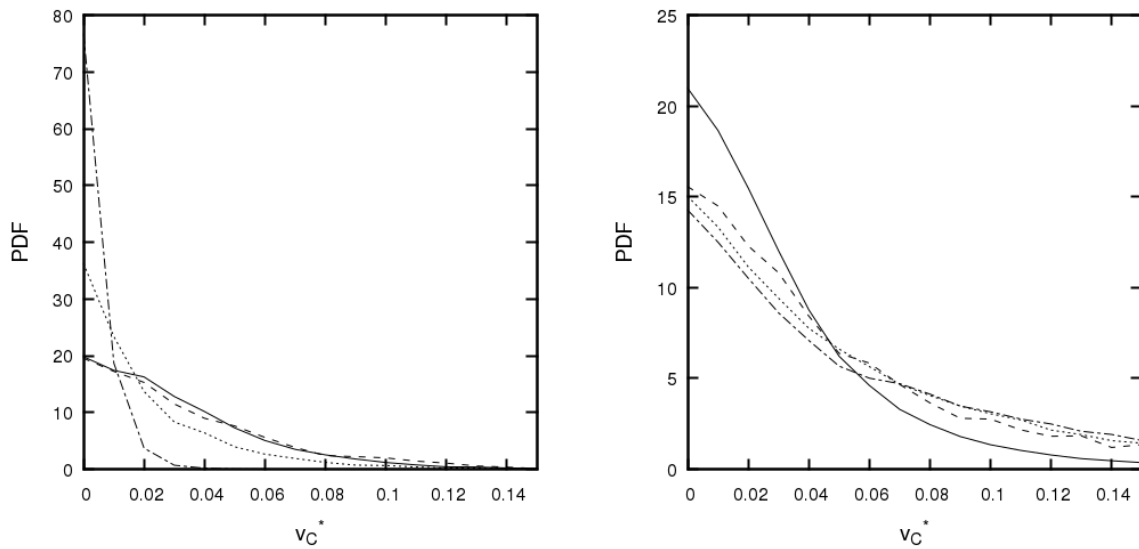

Figure 6: PDFs of collider wall-normal velocity at $St^+ = 0.1$ (left) and $St^+ = 92$ (right). Solid line: bulk flow; dashed: log-law region; dotted: buffer layer; dot-dashed: viscous sublayer.

Figure 8 demonstrates the collision angle (θ) in radians, which is the angle between the colliders' velocity vectors before the collision takes place. In both cases as the wall is approached, the spread and mean collision angle increases. This suggests more chaotic and head-on collisions in those regions. At $St^+ = 0.1$, most of the collisions in the system are due to small deviations from the streamlines (which are locally parallel), and so the likelihood of collision is low. When they do occur, it is a glancing interaction and the exchange of momentum is most likely perpendicular to the direction of motion. Moving towards the wall, the most likely collision angle begins to increase, if only slightly. At the high Stokes number, the probability of more head-on

collisions is increased. This is most true in the viscous sublayer, very close to the channel boundary. In this region, the distribution of collision angles is wide and fairly flat, indicating chaotic interactions in that zone. Moving away from the wall, the collision angles become more well defined and the mean is lowered. In all regions, the mean and spread of angles are much larger than those of the $St^+ = 0.1$ simulation. This is because the trajectories are now governed mainly by particle inertia, and so approach the limit where collision angles are arbitrary. These findings agree with those of Choi et al. [20] who studied particle collisions in isotropic turbulence.
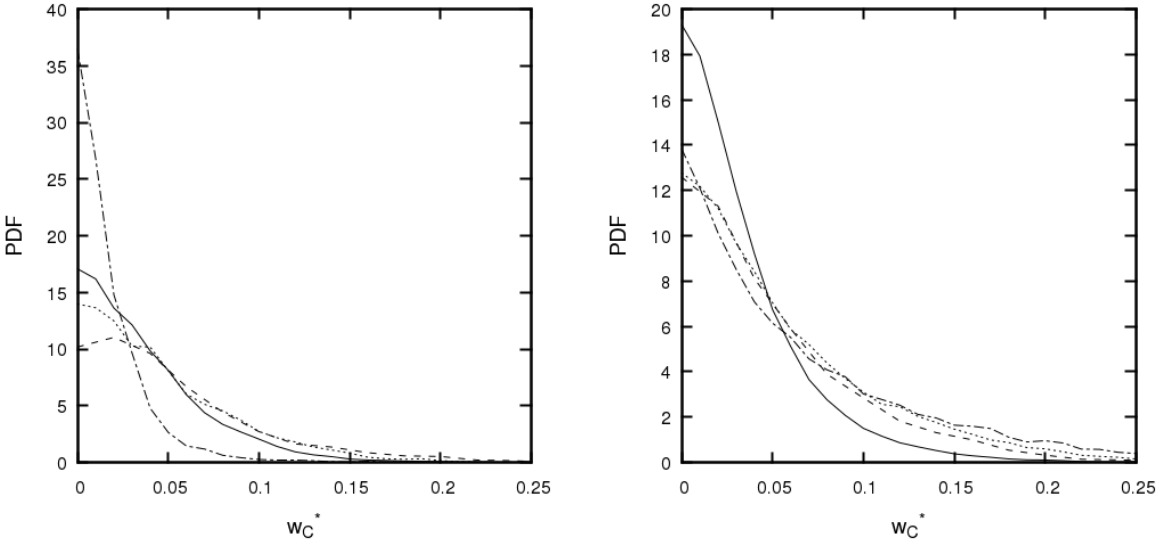

Figure 7: PDFs of collider spanwise velocity at $St^+ = 0.1$ (left) and $St^+ = 92$ (right). Solid line: bulk flow; dashed: log-law region; dotted: buffer layer; dot-dashed: viscous sublayer.
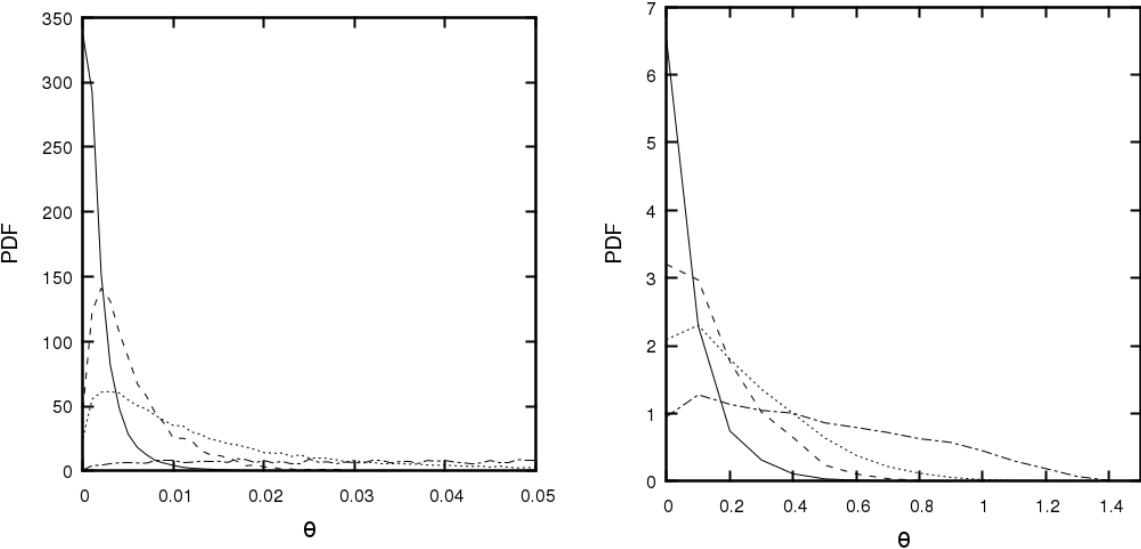

Figure 8: PDFs of angle between colliders at $St^+ = 0.1$ (left) and $St^+ = 92$ (right). Solid line: bulk flow; dashed: log-law region; dotted: buffer layer; dot-dashed: viscous sublayer.
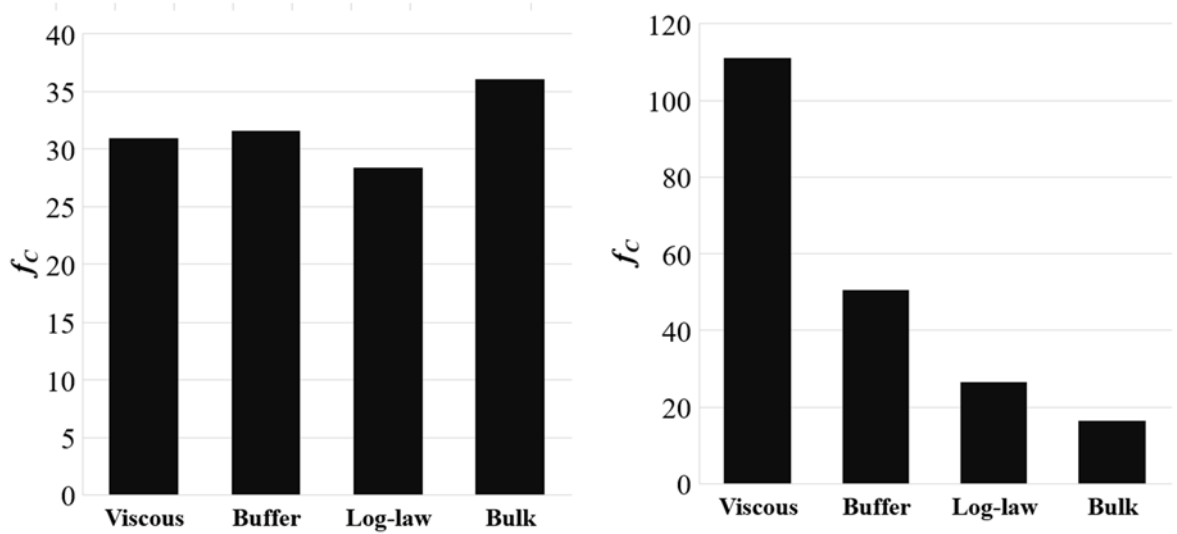
Figure 9: Mean collision rate density (f_C) at $St^+ = 0.1$ (left) and $St^+ = 92$ (right) for each channel flow region.

One final quantity of importance is the collision rate. The nature of this study is such that collision behaviour in different channel flow regions is compared, and so the collision frequency within each of these was calculated and compared. Because each region has a different volume, we have normalised by the length of the region to obtain a collision rate density, defined as $f_C = N_C(r)/(N_{\Delta t^*} L_R^*)$. Here, f_C is the collision rate density, $N_C(r)$ the total number of collisions across the averaging period in a particular region, $N_{\Delta t^*}$ the number of averaging timesteps ($N_{\Delta t^*} = 10^4$) and L_R the length of the region. The results of this analysis are presented in Fig. 9. Evidently, for $St^+ = 0.1$ the collision rate density is relatively homogenous across the four regions, with a slight increase in the bulk. This is expected, given the evenly distributed particle concentration. The $St^+ = 92$ particle set displays an obvious skew towards collisions taking place in the near-wall regions, with most collisions occurring in the viscous sublayer. Here, since particles are driven to these locations due to turbophoresis, increased local concentration and turbulence levels encourage more particle interactions. Another interesting observation is that in the bulk region, particles with $St^+ = 0.1$ actually undergo more collisions than those with $St^+ = 92$. This is likely due to reduced concentrations in this region for the inertial particles.

4. Conclusions

Interparticle collision statistics in a turbulent channel flow have been obtained using a highly accurate direct numerical simulation and Lagrangian particle tracking. Particles were randomly dispersed within a $Re_\tau = 180$ flow, and various interaction statistics were gathered and analysed in an effort to elucidate particle-particle collision dynamics in different regions of the flow.

A validation was performed for both the continuous phase and discrete phase solvers, comparing to pre-existing, well regarded datasets. Excellent accuracy was obtained in both cases.

Simulations were carried out at two shear Stokes numbers, $St^+ = 0.1$ and $St^+ = 92$, representing tracer particles and highly inertial particles, respectively. Concentration profiles indicated turbophoresis taking place for the high Stokes

particle set, whereas the low Stokes particles remained fairly homogeneously distributed. A slight increase around the channel centrel for the high Stokes particles can be explained by particles which had insufficient energy to migrate to the near-wall regions, where they would be encouraged towards the solid boundary.

The greatest spread of streamwise velocities was found to be in the buffer layer in both particle cases, but tracer particles in the viscous sublayer were observed to have much more well defined pre-collision velocities than the inertial particles. This is to be expected as the inertial particles travel from higher layers into this region, but retain their increased velocities. This would not be the case with tracer particles which have very low slip velocities.

For the wall-normal component, the two particle sets had opposite behaviours. Inertial particles possess a spread of velocities in the near-wall regions, whereas in the bulk velocities are more well-defined. For the tracer-like particles, the definition was observed close to the wall. Similar observations were made for the spanwise component; for the low Stokes number particles the greatest spread of spanwise velocities was observed to be in the log-law region.

Collision angles were found to be more representative of head-on collisions for inertial particles, and more glancing for tracer-like particles. In both cases, these angles were larger and more widely distributed closer to the wall. Finally, collision rate densities for each region were compared, the greatest being found for the $St^+ = 92$ case in the viscous sublayer. This is expected due to the increased particle concentration, wall collisions and turbulence in that region.

This work has compared the effects of two Stokes number particles, outside the range usually studied, on particle-particle collisions in turbulent channel flows in order to focus solely on inertial effects. However, further work will determine how these findings differ with particles in the intermediate range, wherein preferential concentration drives near-wall particle density to much higher values, encouraging more collisions.

Acknowledgements

References

1. M.P. Short, D. Hussey, B.K. Kendrick, T.M. Besmann, C.R. Stanek and S. Yip. Multiphysics modeling of porous CRUD deposits in nuclear reactors. *J. Nucl. Mater.*, 443: 579-587, 2013.
2. H.M. Blackburn, N.N. Mansour and B.J. Cantwell. Topology of fine-scale motions in turbulent channel flow. *J. Fluid Mech.*, 310: 269-292, 1996.
3. M.S. Chong, A.E. Perry and B.J. Cantwell. A general classification of three-dimensional flow fields. *Phys. Fluids*, 2: 765-777, 1990.
4. M.W. Reeks. The transport of discrete particles in inhomogeneous turbulence. *J. Aerosol Sci.*, 14: 729-739, 1983.
5. C. Marchioli and A. Soldati. Mechanisms for particle transfer and segregation in a turbulent boundary layer. *J. Fluid Mech.*, 468: 283-315, 2002.
6. I. Rouson and J.K. Eaton. On the preferential concentration of solid particles in

turbulent channel flow. *J. Fluid Mech.*, 428: 149-169, 2001.

7. S. Elghobashi. On predicting particle-laden turbulent flows. *Appl. Sci. Res.*, 52: 309-329, 1994.

8. U.M. Bäbler, S.A. Moussa, M. Soos and M. Morbidelli. Structure and kinetics of shear aggregation in turbulent flows. I. Early stage of aggregation. *Langmuir*, 26: 13142-13152, 2010.

9. T. Tanaka and Y. Tsuji. Numerical simulation of gas-solid two-phase flow in a vertical pipe: On the effect of interparticle collision. *Gas-Solid Flows.*, 121: 123-128, 1991.

10. B. Oesterle and A. Petitjean. Simulation of particle-to-particle interactions in gas-solid flow. *Int. J. Multiph. Flow.*, 19: 199-211, 1993.

11. A.W. Vreman. Turbulence characteristics of particle-laden pipe flow. *J. Fluid Mech.*, 584: 235-279, 2007.

12. Y. Li, J.B. McLaughlin, K. Kontomaris and L. Portela. Numerical simulation of particle-laden turbulent channel flow. *Phys. Fluids*, 13: 2957-2967, 2001.

13. J.G.M. Kuerten and A.W. Vreman. Effect of droplet interaction on droplet-laden turbulent channel flow. *Phys. Fluids*, 27: 053304, 2015.

14. L. Schiller and Z. Naumann. A drag coefficient correlation. *Z. Ver. Deutsch. Ing.*, 77: 318-320, 1933.

15. P.G. Saffman. The lift on a small sphere in a slow shear flow. *J. Fluid Mech.*, 22: 385-400, 1965.

16. H.M. Blackburn, N.N. Mansour and B.J. Cantwell. Topology of fine-scale motions in turbulent channel flow. *J. Fluid Mech.*, 310: 269-292, 1996.

17. K.D. Squires and J.K. Eaton. Particle response and turbulence modification in isotropic turbulence. *Phys. Fluids*, 2: 1191-1203, 1990.

18. A.W. Vreman and J.G.M. Kuerten. Comparison of direct numerical simulation databases of turbulent channel flow at $\mathrm{Re}_\tau = 180$. *Phys. Fluids*, 26: 015102, 2014.

19. C. Marchioli, A. Soldati, J.G.M. Kuerten, B. Arcen, A. Tanière, G. Goldensoph, K.D. Squires, M.F. Cargnelutti and L.M. Portela. Statistics of particle dispersion in direct numerical simulations of wall-bounded turbulence: Results of an international collaborative benchmark test. *Int. J. Multiph. Flow*, 34: 879-893, 2008.

20. J. Choi, Y. Park, O. Kwon and C. Lee. Interparticle collision mechanism in turbulence. *Phys. Rev. E*, 93: 013112, 2016.